Journal of Molecular Catalysis A: Chemical 335 (2011) 89–96

Contents lists available at ScienceDirect

Journal of Molecular Catalysis A: Chemical

journal homepage: www.elsevier.com/locate/molcata

Electrochemical performance of carbon nanotube-supported cobalt phthalocyanine and its nitrogen-rich derivatives for oxygen reduction

Zhanwei Xu, Hejun Li*, Gaoxiang Cao, Qinglin Zhang, Kezhi Li, Xueni Zhao

C/C Composites Research Center, State Key Laboratory of Solidification Processing, Northwestern Polytechnical University, Xi'an 710072, PR China

ARTICLE INFO

Article history:
Received 23 September 2010
Received in revised form 9 November 2010
Accepted 15 November 2010
Available online 23 November 2010

Keywords:
Catalytic activity
Phthalocyanine
Nitrogen
Carbon nanotubes
Oxygen reduction

ABSTRACT

Multiwalled carbon nanotube (MWCNT)-supported cobalt phthalocyanine (CoPc), cobalt tetrapyridinoporphyrazine (CoTAP), and cobalt tetrapyrazinoporphyrazine (CoPTpz) assemblies are prepared by solid phase synthesis method. The products are characterized by infrared spectroscopy, scanning and transmission electron microscopy and UV–vis spectroscopy. The electrocatalytic activity of the obtained MWCNT-supported CoPc, CoTAP and CoPTpz assemblies is measured by rotating disk electrode techniques and cyclic voltammetry in an oxygen-saturated 0.1 M KOH. The results show that MWCNT-supported CoPc shows a two-step, two-electron process for the reduction of oxygen reduction (ORR), whereas MWCNT-supported CoTAP and CoPTpz electrodes exhibit a one-step, four-electron pathway for ORR, indicating that N atoms in the backbone of the compounds strongly affect the catalytic activity of MWCNT-supported CoPc derivative assemblies. The MWCNT-supported CoTAP and CoPTpz assemblies have higher activity to oxygen reduction than that of MWCNT-supported CoPc attributed to their different catalytic mechanisms to ORR.

1. Introduction

The oxygen reduction reaction (ORR) in acidic and alkaline solution has aroused much interest in the fields of electrocatalysis, especially in fuel cells [1,2], air-breathing cathodes [3,4] and metal-air batteries [5]. Efficient ORR electrocatalysts play a key role in these applications [1,2]. Transition metal phthalocyanine (MPc) is an interesting kind of compound with a conjugated ligand and a transition central metal ion. A delocalized conjugated π bond in the molecule makes MPc liable to oxidation and reduction [6–8], which is an advantage for the compound to be used as electrocatalysts [9]. MPc compounds used as catalysts for ORR have been paid much attention [10–20], especially, cobalt phthalocyanine (CoPc) [11–17].

Carbon nanotubes (CNTs), as a new member of the carbon derivatives [21], have unique one-dimensional nanostructure, high surface areas, high thermal conductivity, and excellent chemical and thermal stability [22,23], all of which benefit the support of catalyst. CNT-supported MPc compounds used as catalysts for ORR have attracted much interest [24–26]. It has been reported that nitrogen atoms in the backbone strongly affect the properties of MPc derivatives [27–31]. However, to the best of our knowledge, few work related to the properties of CNTs decorated with diverse nitrogen atoms in the backbone of MPc derivatives for ORR has been shown. In this paper, with an attempt to show the effects of nitrogen atoms in the backbone of CoPc derivatives on the electrochemical performance of MWCNT-supported CoPc derivatives, we prepared MWCNT-supported CoPc, cobalt tetrapyridinoporphyrazine (CoTAP) and cobalt tetrapyrazinoporphyrazine (CoPTpz) assemblies, and used them as catalysts for ORR (the structures of CoPc, CoTAP and CoPTpz are shown in Fig. 1).

2. Experimental

MWCNT-supported CoPc, CoTAP and CoPTpz were prepared by solid-phase synthesis method [32], and used as catalysts for ORR. Rotating disk electrode (RDE) techniques and cyclic voltammetry (CV) measurements were used to evaluate their electrocatalytic activity for ORR.

2.1. Materials

Acid functionalized multiwalled-carbon nanotubes (AF-MWCNTs) were obtained from Chengdu Organic Chemical Co, Ltd., Chinese Academy of Sciences. The typical diameter of MWCNTs was confirmed by using transmission electron microscopy (TEM) with around 20 nm in outer diameter. O-phthalic anhydride, pyridine-2,3-dicarboxylic acid, 2,3-pyrazinedicarboxylic acid and Nafion solution (5 wt% in ethanol) were obtained from Alfa Aesar

* Corresponding author. Tel.: +86 29 88495004; fax: +86 29 88492642.
E-mail address: lihejun@nwpu.edu.cn (H. Li).

1381-1169/$ – see front matter © 2010 Elsevier B.V. All rights reserved.
doi:10.1016/j.molcata.2010.11.018

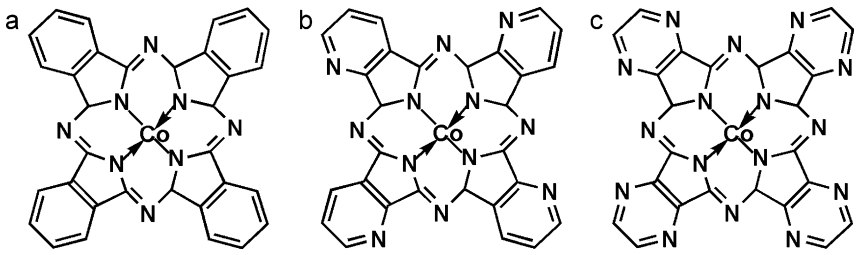

Fig. 1. Structures of (a) CoPc, (b) CoTAP and (c) CoPTpz.

Co., and all other reagents are of analytical grades and used without further purification.

2.2. Synthesis of catalysts

MWCNT-supported CoPc, CoTAP and CoPTpz assemblies were prepared by a solid-phase synthesis method in a muffle furnace [32]. For preparing MWCNT-supported CoTAP assemblies, a mixture of 0.50 g AF-MWCNTs, 1.20 g pyridine-2,3-dicarboxylic acid, 2.00 g urea, 1.50 g $CoCl_2{\cdot}6H_2O$, and 0.20 g $(NH_4)_2Mo_2O_7$ was ground. Next, it was transferred in a 100 ml crucible, heated in a muffle furnace at 140 °C for 1.5 h and subsequently at 270 °C for 3 h under ambient air conditions. After being cooled to room temperature, the product was washed with water, acetone, and methyl alcohol in sequence. The precipitates were dried under vacuum at 70 °C overnight. MWCNT-supported CoPc and CoPTpz assemblies were synthesized by the similar method, and CoPc, CoTAP, and CoPTpz as the reference were synthesized under the same conditions but without the AF-MWCNTs (details are shown in Supporting Information).

2.3. Characterization

Scanning electron microscopy (SEM) images of the products were obtained using a JEOL JSM-6700 field emission scanning electron microscope. Infrared spectroscopy (IR) spectra of the assemblies were measured by a Germany EQUINOX 55spectrameter (KBr pellets) in the 4000–400 cm^{-1} range. TEM images of the products were obtained by a JEOL JEM-3010 high-resolution TEM. The X-ray diffraction (XRD) patterns of the assemblies were detected by a Rigaku (Tokyo, Japan) D/max-2400 X-ray diffractometer with Cu Kα radiation. UV–vis spectra of the sample solution (DMSO) were measured by using Perkin-Elmer Lambda 40 UV–visible spectrometer.

2.4. Electrochemistry

The glassy carbon electrode (GC, 3 mm in diameter) was polished by ~0.5 μm alumina slurry, and then washed ultrasonically in distilled water for 3 min and in acetone for 3 min. The cleaned GC was dried in air. 10 μL of a 2 g L^{-1} obtained MWCNT-supported assembly (ethanol) suspension was pipetted onto the GC. After evaporation of ethanol, 10 μL of a diluted Nafion solution (5 wt% in ethanol) was put on the top of the product suspension, and then dried in air to hold the attachment of the product to the electrode surface. The bulk CoPc and CoTAP coated GCs are prepared by similar procedures.

RDE and CV measurements were performed with a CorrTest electrochemical work station (CS310 Wuhan CorrTest Instrument Co. Ltd.) in a conventional three-electrode cell using the coated GC (3 mm diameter) as the working electrode, platinum foil as the auxiliary electrode, and Ag/AgCl as reference electrode. 0.1 M KOH solutions were used in the experiments. All solutions were de-aerated by bubbling oxygen (or nitrogen) prior to each electrochemical experiment for ~30 min. During the test, the trachea was put on the liquid surface. After finishing this test, the solutions were de-aerated by bubbling oxygen (or nitrogen) again for ~10 min, and then do the next [33].

RDE measurements were done in O_2 saturated solution, with the scan rate of 10 mV s^{-1}. CV measurements were done in N_2/O_2 saturated solution, with the scan rate of 50 mV s^{-1}. Before CV measurements, the electrode was repeatedly potentiodynamic swept from −1.0 to +0.2 V in an oxygen-protected 0.1 M KOH until a steady voltammogram curve was obtained. All the experiments were performed at room temperature.

3. Results and discussion

3.1. Structure analysis

The obtained CoPc/MWCNTs, CoTAP/MWCNTs, and CoPTpz/MWCNTs have uniform capsule-like morphology. The shapes of the obtained CoPc/MWCNTs, CoTAP/MWCNTs and CoPTpz/MWCNTs are similar to that of MWCNTs acting as supports. However, the outer diameter of the as-products is much larger than that of MWCNTs due to deposition of organic compounds on the surface (as shown in Fig. 2).

IR spectra of the obtained products are shown in Fig. 3. AF-MWCNTs show a broad band at ~1712 cm^{-1} assigned to COOH moieties, corresponding to the symmetric C=O stretching. It is interesting to find that very weak peaks around 1728 cm^{-1} can be observed among CoPc/MWCNTs, CoTAP/MWCNTs and CoPTpz/MWCNTs, assigned to COOH moieties shift to high wave number attributed to the formation of the coordination bond between Co of Co-complexes and O of AF-MWCNTs [34]. In addition, the spectra of CoPc/MWCNTs show the Co–N band around

Table 1
IR spectra of AF-MWCNTs, CoL and CoL/MWCNTs.

Samples	C=O	C=N	C=C	C–H	Co–N	Backbone of CoPc
AF-MWCNTs	1712			~1015		
CoPc		1612	1523	1092	913	731
CoPc/MWCNTs	1728	1612	1523	1092	913	731
CoTAP		1666, 1585	1522	1134	923	793, 745
CoTAP/MWCNTs	1728	1666, 1585	1522	1134	923	793, 745
CoPTpz		1631	1516	1120	935	755
CoPTpz/MWCNTs	1728	1631	1516	1120	935	755

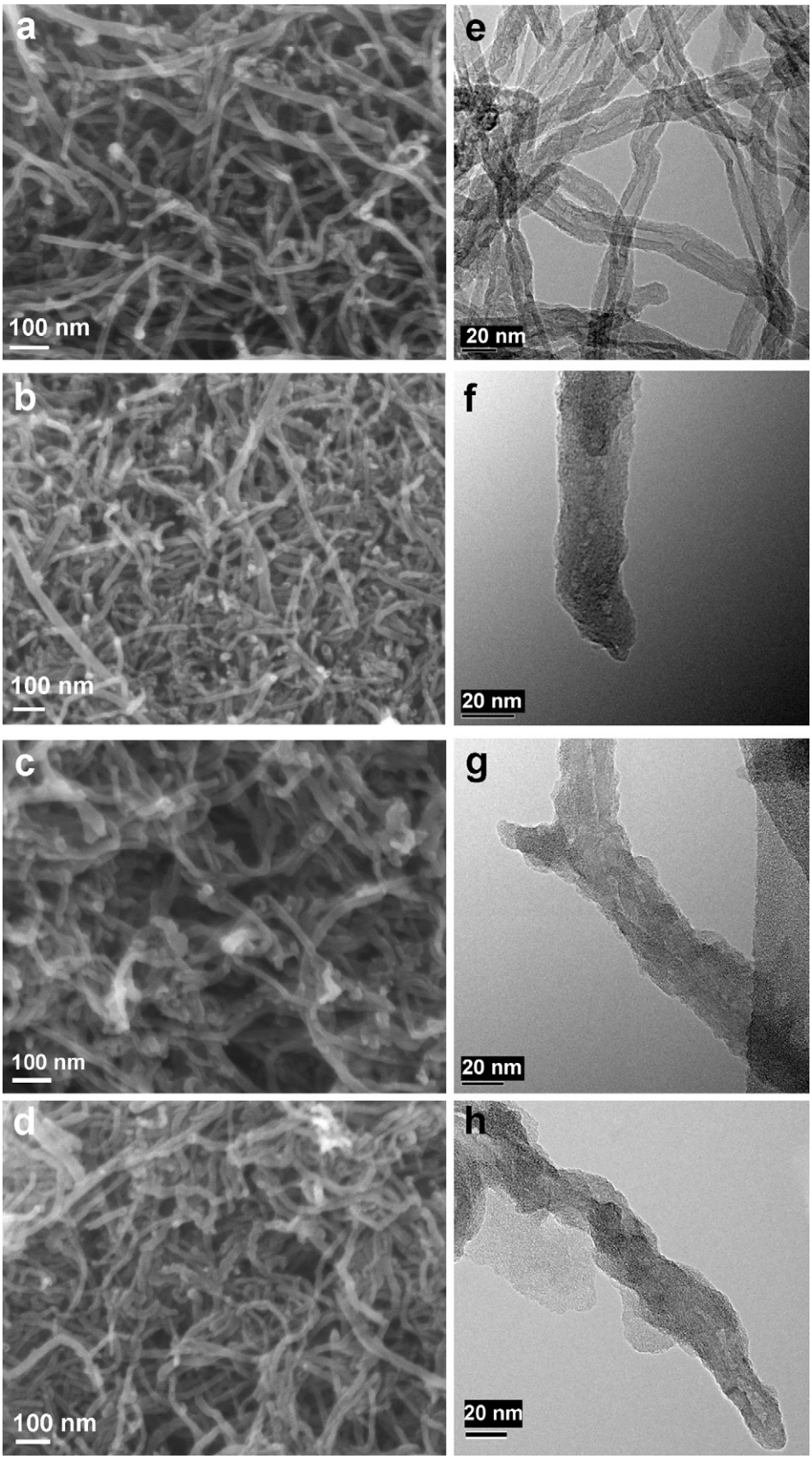

Fig. 2. SEM images of (a) MWCNT supports, (b) CoPc/MWCNTs, (c) CoTAP/MWCNTs and (d) CoPTpz/MWCNTs. TEM images of (e) MWCNT supports, (f) CoPc/MWCNTs, (g) CoTAP/MWCNTs and (h) CoPTpz/MWCNTs.

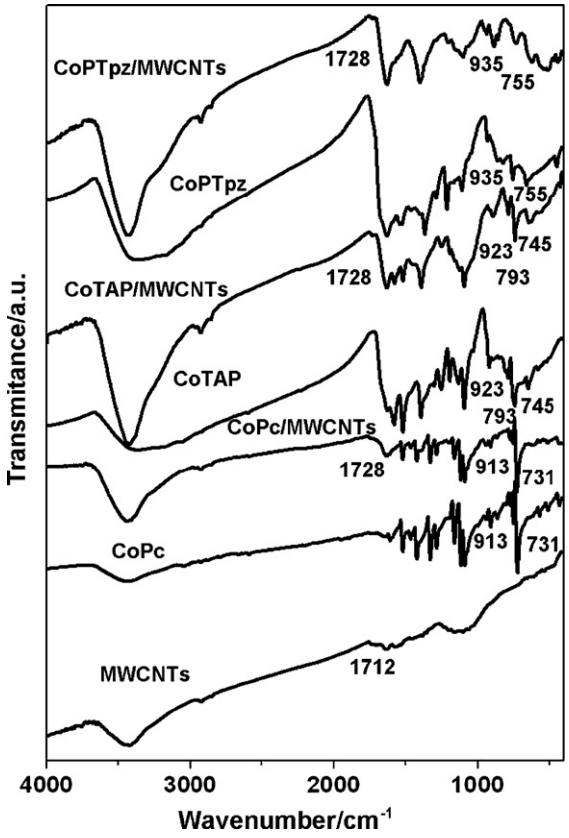

Fig. 3. IR spectra of MWCNT supports, CoPc, CoPc/MWCNTs, CoTAP, CoTAP/MWCNTs, CoPTpz, and CoPTpz/MWCNTs.

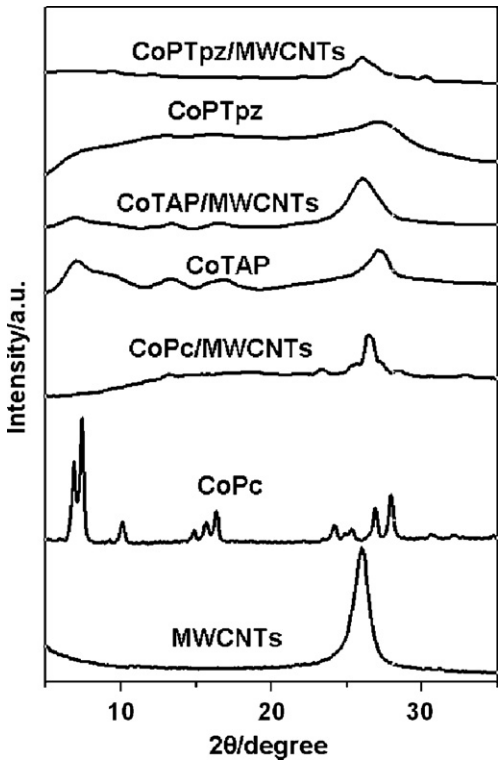

Fig. 4. XRD patterns of MWCNT supports, CoPc, CoPc/MWCNTs, CoTAP, CoTAP/MWCNTs, CoPTpz, and CoPTpz/MWCNTs.

913 cm^{-1}, and the band assigned to the backbone of CoPc around 731 cm^{-1}. The spectra of CoTAP/MWCNTs show the Co–N band around 923 cm^{-1}, and the band assigned to the backbone of CoTAP around 793 and 745 cm^{-1}. The spectra of CoPTpz/MWCNTs show the Co–N band around 935 cm^{-1}, and the band assigned to the backbone of CoPTpz around 755 cm^{-1}. The spectra of CoPc/MWCNTs, CoTAP/MWCNTs and CoPTpz/MWCNTs also show other bands corresponding to that of CoPc, CoTAP and CoPTpz, respectively [31] (as shown in Fig. 3 and Table 1). IR spectra provide evidence to the formation of CoPc, CoTAP and CoPTpz assemblies.

The XRD patterns of MWCNT support, bulk CoPc, CoPc/MWCNTs, bulk CoTAP, CoTAP/MWCNTs, bulk CoPTpz and CoPTpz/MWCNTs are shown in Fig. 4. The diffraction pattern of MWCNT shows typical peak at $2\theta = 25.76^\circ$, corresponding to the (0 0 2) reflection [35]. The XRD patterns of bulk CoPc show seven peaks at $2\theta = 7.19^\circ$, 10.02°, 15.58°, 24.23°, 25.29°, 26.74° and 27.93°. The XRD patterns of CoPc/MWCNTs show three peaks, one of which is a broaden band between 14.00° and 19.00°, the others are the peaks at $2\theta = 23.22^\circ$ and 25.76°. Among them, the peak at $2\theta = 25.76^\circ$ is assigned to MWCNTs. Compared to the XRD patterns of bulk CoPc, the peaks of CoPc on the surface of MWCNTs become weaker or disappear, indicating that CoPc cannot stack into a long-range ordered state attributed to the limitation of the number of CoPc molecules in nanosized CoPc [36]. Compared with the XRD patterns of bulk CoTAP displaying four peaks at 7.00°, 13.27°, 17.10° and 27.29°, that of CoTAP/MWCNTs show four peaks at 7.00°, 13.27°, 17.10° and 25.76°. Among them, the three peaks at 7.00, 13.27, and 17.10° are assigned to CoTAP. The largest and broadest peak around 25.76° is the overlap of the peaks at 25.76° of MWCNTs and 27.29° of CoTAP. The XRD patterns of bulk CoPTpz have one peak at 27.90°, and CoPTpz/MWCNTs have a broaden peak in the range between 25.0° and 28.5°, which is the overlap of the peaks at 25.76° of MWCNTs and 27.90° of CoPTpz (Table 2). The observed broadness of the peaks for all of Co-complexes/MWCNTs XRD patterns suggests that they are all in semi-crystalline form [37].

3.2. Oxygen reduction analysis

To investigate the electrochemical performance of MWCNT-supported CoPc assemblies immobilised onto a glass carbon electrode (i.e. GC/CoPc/MWCNTs), MWCNT-supported CoTAP assemblies immobilised onto a glass carbon electrode (GC/CoTAP/MWCNTs), and MWCNT-supported CoTAP assemblies immobilised onto a glass carbon electrode (GC/CoPTpz/MWCNTs), we used the bare glass carbon electrode (GC) and seven coated GCs as the working electrodes. Fig. 5 shows CV response of N_2/O_2 saturated alkaline solution at the bare GC and seven coated GCs, including: MWCNT immobilised onto a GC (GC/MWCNTs), GC/CoPc/MWCNTs, GC/CoTAP/MWCNTs, GC/CoPTpz/MWCNTs, bulk CoPc, CoTAP and CoPTpz immobilised onto GCs (GC/CoPc, GC/CoTAP and GC/CoPTpz), respectively. The peak potential (E_p) and peak current (I_p) for ORR in 0.1 M KOH solution are shown in Table 3. Generally, CVs of GC/MWCNTs, GC/CoPc/MWCNTs, GC/CoTAP/MWCNTs and GC/CoPTpz/MWCNTs display higher background currents than that of bare GC, GC/CoPc, GC/CoTAP and GC/CoPTpz. All used electrodes exhibit ORR activities in alkaline

Table 2
XRD data of AF-MWCNTs, CoL and CoL/MWCNTs.

Samples	Corresponding 2θ (°)
AF-MWCNTs	25.76
CoPc	7.19, 10.02, 15.58, 24.23, 25.29, 26.74, 27.93
CoPc/MWCNTs	14.00, 19.00, 23.22, 25.76 (broaden peak)
CoTAP	7.00, 13.27, 17.10, 27.29
CoTAP/MWCNTs	7.00, 13.27, 17.10, 25.76 (broaden peak)
CoPTpz	27.90
CoPTpz/MWCNTs	25.00–28.50 (broaden peak)

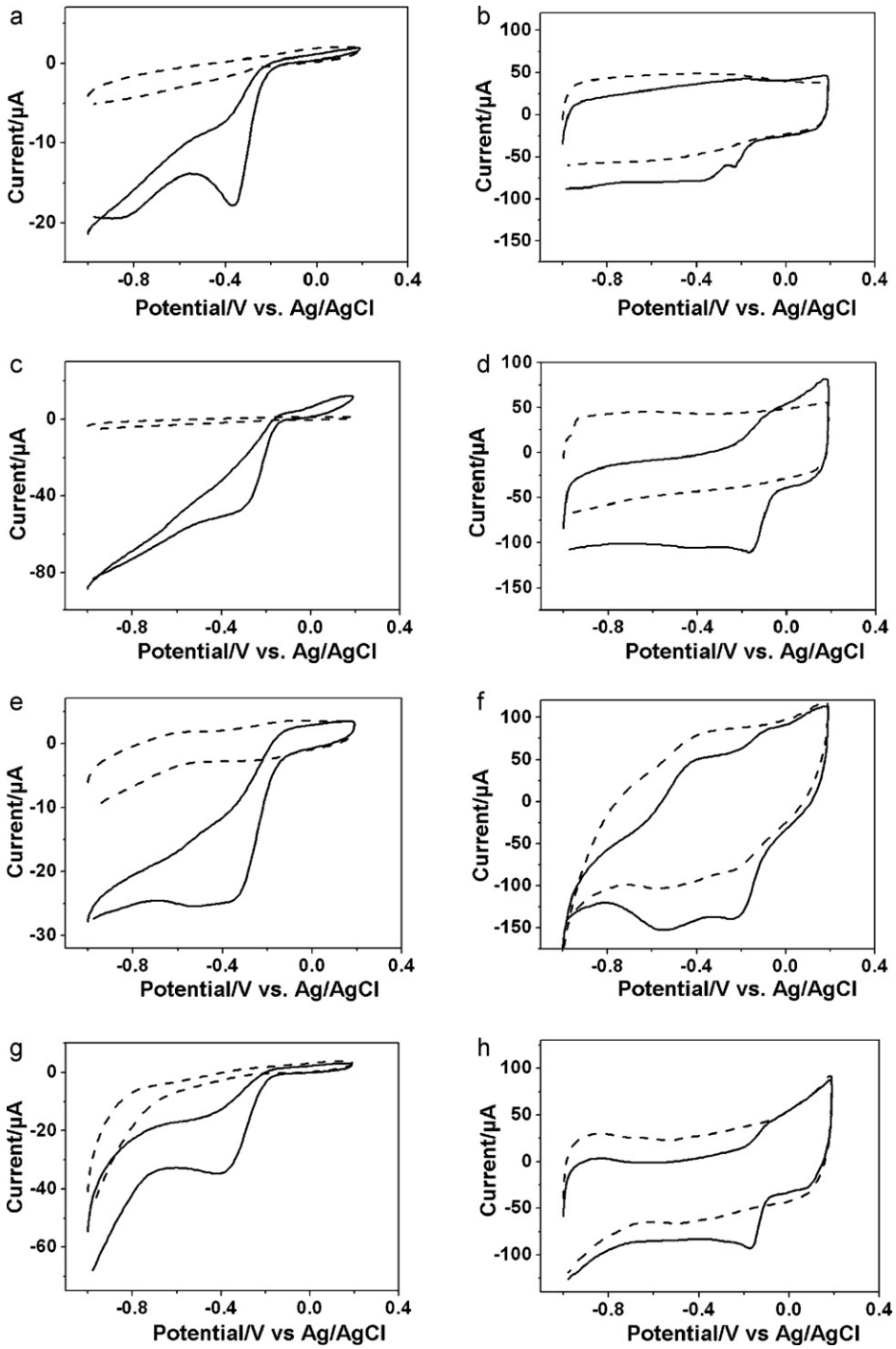

Fig. 5. CVs for ORR at (a) the GC electrodes, (b) GC/MWCNTs, (c) GC/CoPc, (d) GC/CoPc/MWCNTs, (e) GC/CoTAP, (f) GC/CoTAP/MWCNTs, (g) GC/CoPTpz, and (h) GC/CoPTpz/MWCNTs in nitrogen protected (dash curves) or oxygen-saturated 0.1 M KOH (solid curves) at the scan rate of 50 mV s^{-1}; GC electrode area: 0.0707 cm^2.

solution by comparing CV responses between O_2 and N_2 saturated 0.1 M KOH solution. In 0.1 M KOH solution, CV of the bare GC shows a reduction peak (−0.36 V vs. Ag/AgCl, 0.1 M KOH) in O_2 saturated solution (Fig. 5a), consistent with the result that Kullapere et al. reported [38]. For GC/MWCNTs in Fig. 5b, an oxygen reduction peak (−0.23 V) with a strong background current was observed as compared to bare GC, which was attributed to larger specific surface area caused by high surface-to-volume ratio. For GC/CoPc and GC/CoPc/MWCNTs (Fig. 5c and d), the oxygen reduction peaks were at similar positions (−0.21 V for GC/CoPc, −0.18 V for GC/CoPc/MWCNTs), however, the peak current (−81.7 μA) of the GC/CoPc/MWCNTs is 0.8 times larger than that (−46.6 μA) of GC/CoPc attributed to higher surface-to-volume ratio of nanosized CoPc. In comparison to CVs of GC/CoTAP exhibiting a broaden peak around −0.38 V, it is interesting to find that CV response of GC/CoTAP/MWCNTs has two peaks at −0.57 and −0.20 V, like splitted peaks of the broaden peak. In addition, the peak currents corresponding to the peak potential at −0.57 and −0.23 V are −152.0 and −139.1 μA, which were 5.0 and 4.5 times larger than that GC/CoTAP (as shown in Fig. 5e and f). As to GC/CoPTpz and GC/CoPTpz/MWCNTs (Fig. 5g and h), the oxygen reduction peaks were at −0.36 and −0.18 V, respectively. The peak current

Table 3
Comparison of peak potential (E_p) and peak current (I_p) for ORR on bare and seven coated GCs.

Electrodes	E_p (V)	I_p (μA)
GC	−0.36	−17.3
GC/MWCNTs	−0.23	−61.5
GC/CoPc	−0.21	−46.6
GC/CoPc/MWCNTs	−0.18	−81.7
GC/CoTAP	−0.38	−25.5
GC/CoTAP/MWCNTs	−0.57	−152.0
	−0.20	−139.1
GC/CoPTpz	−0.36	−38.0
GC/CoPTpz/MWCNTs	−0.18	−115.0

(−115.0 μA) of GC/CoPTpz/MWCNTs is about 2.0 times larger than that (−38.0 μA) of GC/CoPTpz.

The electrochemical reduction of O_2 is a multi electron reaction that has two main possible pathways: one involving gain of two electrons to produce H_2O_2, and the other, a direct four-electron pathway to produce water. In alkaline media, the $2e^-$ pathway can be written as [12]:

$$O_2 + H_2O + 2e^- \rightarrow HO_2^- + OH^- \quad (1)$$

The direct $4e^-$ pathway can be written as:

$$O_2 + 2H_2O + 4e^- \rightarrow 4OH^- \quad (2)$$

To obtain maximum energy capacity, it is highly desirable to reduce O_2 via the $4e^-$ pathway.

In order to gain better insight on the ORR electrochemical procedure of GC/CoPc/MWCNTs, GC/CoTAP/MWCNTs and GC/CoPTpz/MWCNTs, the RDE voltammogram for ORR was performed at various rotation rates. The RDE polarization curves are shown in Fig. 6. These polarization curves show current plateaus in the high-polarization rang, which is similar to carbon supported CoPc in 0.1 M NaOH solution [12].

The RDE data were analyzed using the Koutecky–Levich (K–L) equation:

$$\frac{1}{I} = \frac{1}{I_k} + \frac{1}{I_{lim}} \quad (3)$$

$$I_{lim} = 0.62nFD^{2/3}\nu^{-1/6}C_0\omega^{1/2} \quad (4)$$

where I is the total current density, I_k is activation controlled current density, I_{lim} is limiting current density, n is the number of electrons transferred per oxygen molecule, F is Faraday constant (96,500 C mol^{-1}), D is the diffusion coefficient of O_2 in 0.1 M KOH (1.9×10^{-5} cm^2 s^{-1}), C_0 is the concentration of oxygen(1.2×10^{-6} mol cm^{-3}), ν is the viscosity of the electrolyte (1.1×10^{-2} cm^2 s^{-1}), and ω is the rotation rate of the radian [39–44].

The rate of oxygen reduction of the film-modified electrode strongly depends on these processes, including mass transport process of O_2 in the solution, catalytic process at the electrode film/solution interface, and electron diffusion process within the film. The ORR limiting current density is determined by one or more of these processes [45]. The mass transport limiting ORR currents reach at the potential lower than −0.25, −0.30 and −0.27 V (vs. Ag/AgCl) on the electrodes of CoPc/MWCNTs, CoTAP/MWCNTs, and CoPTpz/MWCNTs, respectively. While the mixed mass transport and kinetic controlled range from −0.25 to −0.15 V on the CoPc/MWCNTs, from −0.30 to −0.18 V on the CoTAP/MWCNTs, and from −0.28 to −0.15 V on the CoPTpz/MWCNTs. The steady-state catalytic current densities at the MWCNT-supported CoTAP and CoPTpz were found to be ~1.8 times as that of the MWCNT-supported CoPc electrode over a large potential range (as shown in Fig. 6.).

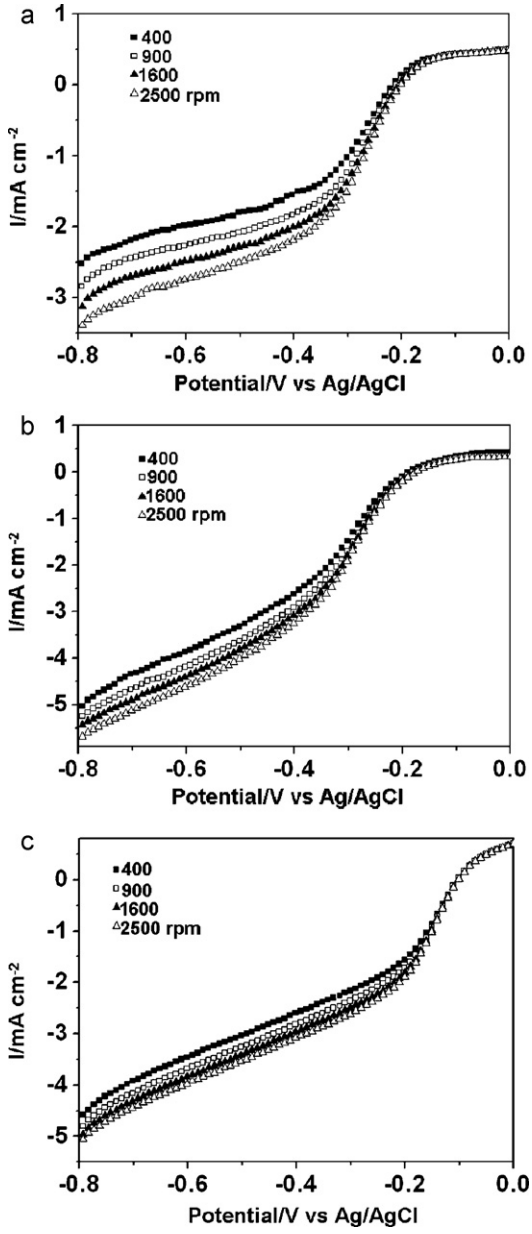

Fig. 6. RDE polarization curves at different rotation rates for ORR on: (a) GC/CoPc/MWCNTs, (b) GC/CoTAP/MWCNTs and (c) GC/CoPTpz/MWCNTs at the scan rate of 10 mV s^{-1}.

According to the K–L equation and the results of Fig. 6, the K–L plots of I^{-1} vs. $\omega^{-1/2}$ at fixed potentials were drawn and shown in Fig. 7. It can be seen that the transferred electron number per oxygen molecule on the GC/CoPc/MWCNTs, GC/CoTAP/MWCNTs and GC/CoPTpz/MWCNTs electrodes is 1.7–1.8, 3.6–3.9, and 3.6–3.9, respectively. Therefore, GC/CoPc/MWCNTs shows a two-step, two-electron process for oxygen reduction (Fig. 7a), which is similar to carbon-supported CoPc reported by Chen et al. [12], whereas GC/CoTAP/MWCNTs and GC/CoPTpz/MWCNTs electrodes exhibit a one-step, four-electron pathway for the ORR (Fig. 7b and c). On the basis of the analysis above, the GC/CoTAP/MWCNTs and GC/CoPTpz/MWCNTs electrodes exhibit better electrocatalytic activity for ORR than the GC/CoPc/MWCNTs electrode.

The mechanism of the catalytic reduction of O_2 by CoPc and other MPc derivatives has been demonstrated by Lever, Chen et al. and Sehlotho and Nyokong [11,12,15]. It has shown that the reduction of oxygen catalyzed by MPc is an electron transfer process

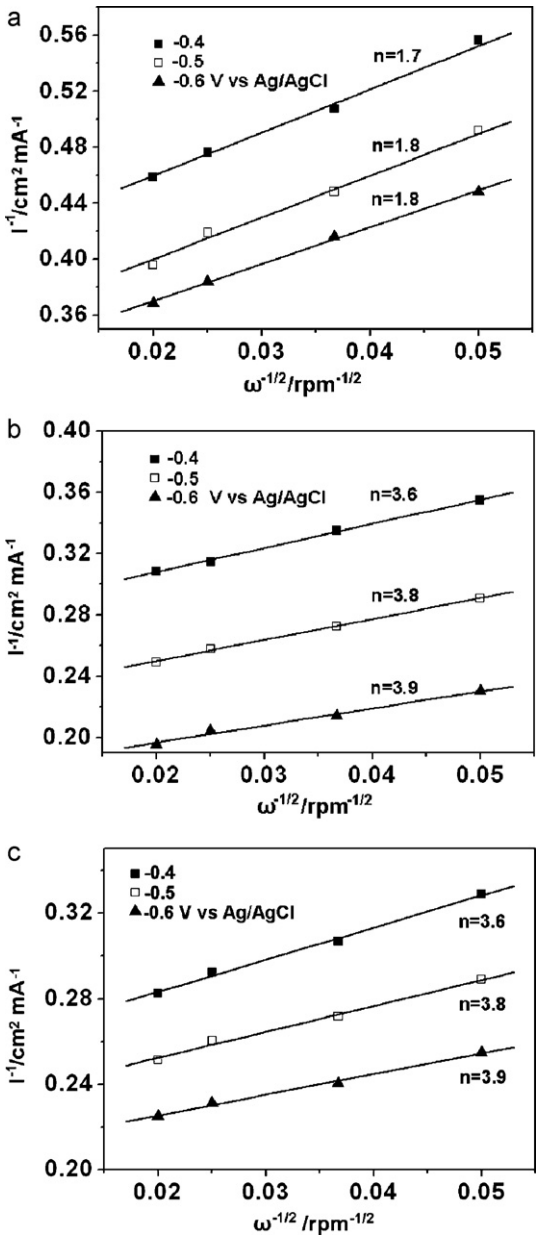

Fig. 7. Plot of I^{-1} vs. $\omega^{-1/2}$ for oxygen reduction on ORR on: (a) GC/CoPc/MWCNTs, (b) GC/CoTAP/MWCNTs and (c) GC/CoPTpz/MWCNTs at potentials −0.4, −0.5, and −0.6 V vs. Ag/AgCl.

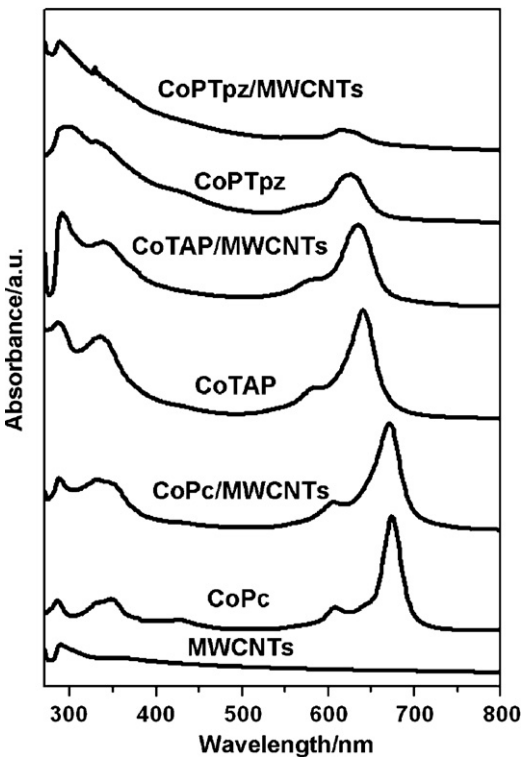

Fig. 8. UV–vis spectra of MWCNT supports, CoPc, CoPc/MWCNTs, CoTAP, CoTAP/MWCNTs, CoPTpz, and CoPTpz/MWCNTs.

[11,46], and MPc electrochemistry in the solution phase is characterized as multiple and often reversible redox processes localized on the metal center or the phthalocyanine ring [11].

UV–vis spectra exhibit external electron transfer process, and are often used to show the electron transitions between the highest occupied molecular orbital (HOMO) and the lowest molecular orbital (LUMO) of the catalysts. To CoPc, the strongest band in the wavelength region of 580–710 nm which is attributed to the π–π transition centered on the macrocycle of CoPc molecules [31,47,48], is the Q band. Another band in the region of 280–360 nm contributed by the backbone of the phthalocyanine ring, is the B band. The UV–vis spectrum of CoPc shows two peaks of Q band at 596 and 672 nm, which are dimer and monomer bands of CoPc, respectively [31]. The Q band of the UV–vis spectra of CoPc/MWCNTs is one prominent broadened peak in the region of 550–690 nm, showing a strong peak at 670 nm attributed to the monomer of CoPc, and a weak peak at 596 nm attributed to the dimer of CoPc. The activity of the Q band is mainly attributed to the monomer because the dimer has little activity. The Q band of CoTAP is within the range of 550–670 nm and two peaks of Q band are at 577 and 638 nm, assigned to the bands of dimer and monomer of CoTAP, respectively. The B band of CoTAP is within the region of 270–370 nm [31]. Compared with CoPc/MWCNTs, the B band absorbance of CoTAP/MWCNTs is much stronger than that of CoPc/MWCNTs, whereas the Q band absorbance of CoTAP/MWCNTs and the intensity of the dimer and monomer of CoTAP/MWCNTs are similar to that of CoPc/MWCNTs. The B and Q bands of CoPTpz are in the region of 270–360 nm, and 580–650 nm, respectively. It is clearly to see that CoPTpz has a relatively strong and broaden B but no significant Q band. And the B bands and Q bands of the electron absorbance of CoPTpz/MWCNTs are similar to that of CoPTpz (as shown in Fig. 8).

CoPc/MWCNTs have relatively strong electron absorbance in Q band but weak in B band. Additionally, N atoms are located in the porphyrin cycle with steric hindrance for O_2 to attach. CoPc on the surface of MWCNTs has one possible active site, that is central metal ion Co^{2+} [11,49]. Adsorption of O_2 is formed via the coordinate bond between the O atom of O_2 and Co^{2+}. Due to the strong strength of the coordinate bond, the desorption of the resultant and unreacted O_2 from the catalyst becomes very difficult. Therefore, MWCNT-supported CoPc has lower activity to oxygen reduction. UV–vis spectra of MWCNT-supported CoTAP and CoPTpz assemblies display strong electron absorbance spectra in Q band. In addition, N atoms are located in the out ring of the molecules, providing sites for O_2 to attach. The chemisorption of O_2 on CoTAP and CoPTpz can form through π–π interaction between the delocalized π electrons of O_2 and delocalized π electrons of TAP and PTpz ring. It is easy for both the adsorption of O_2 and the desorption of resultant and un-reacted O_2 from the catalyst. Therefore, the MWCNT-supported CoTAP and CoPTpz assemblies have higher activity to oxygen reduction than that of MWCNT-supported CoPc assemblies attributed to their different catalytic mechanisms to ORR.

4. Conclusions

MWCNT-supported CoPc, CoTAP and CoPTpz assemblies were fabricated by solid phase synthesis method in a muffle furnace and used as catalysts for the reduction of oxygen. MWCNT-supported CoPc shows a two-step, two-electron process for ORR, whereas MWCNT-supported CoTAP and CoPTpz electrodes exhibit a one-step, four-electron pathway for ORR. The MWCNT-supported CoTAP and CoPTpz assemblies have higher activity to oxygen reduction than that of MWCNT-supported CoPc assemblies attributed to their different catalytic mechanisms to ORR.

Acknowledgement

This work has been supported by the National Natural Science Foundation of China under Grant No. 50832004, the Research Fund of State Key Laboratory of Solidification Processing (NWPU), China (Grant No. 25-TZ-2009), and the Doctorate Foundation of Northwestern Polytechnical University.

Appendix A. Supplementary data

Supplementary data associated with this article can be found, in the online version, at doi:10.1016/j.molcata.2010.11.018.

References

[1] S. Maldonado, K.J. Stevenson, J. Phys. Chem. B 109 (2005) 4707–4716.
[2] K.P. Gong, F. Du, Z.H. Xia, M. Durstock, L. Dai, Science 323 (2009) 760–764.
[3] C.Y. Chen, P. Yang, J. Power Sources 123 (2003) 37–42.
[4] J.F. Ma, Y.N. Liu, P. Zhang, J. Wang, Electrochem. Commun. 10 (2008) 100–102.
[5] E. Yeager, J. Mol. Catal. 38 (1986) 5–25.
[6] M. Kimura, T. Kuroda, K. Ohta, K. Hanabusa, H. Shirai, N. Kobayashi, Langmuir 19 (2003) 4825–4830.
[7] N. Nishiyama, A. Iriyama, W.D. Jang, K. Miyata, K. Itaka, Y. Inoue, H. Takahashi, Y. Yanagi, Y. Tamaki, H. Koyama, K. Kataoka, Nat. Mater. 4 (2005) 934–940.
[8] A. Sorokin, J.L. Séris, B. Meunier, Science 268 (1995) 1163–1166.
[9] M. Stantney, W. Ham, Chem. Rev. 104 (2004) 4271–4301.
[10] J.H. Zagal, Coord. Chem. Rev. 119 (1992) 89–136.
[11] A.B.P. Lever, J. Porphyrins Phthalocyanines 3 (1999) 488–499.
[12] R.R. Chen, H.X. Li, D. Chu, G.F. Wang, J. Phys. Chem. C 113 (2009) 20689–20697.
[13] M. Özer, A. Altındal, A.R. Özkaya, Ö. Bekaroğlu, Dalton Trans. (2009) 3175–3181.
[14] İ. Koç, M. Özer, A.R. Özkaya, Ö. Bekaroğlu, Dalton Trans. (2009) 6368–6376.
[15] N. Sehlotho, T. Nyokong, J. Electroanal. Chem. 595 (2006) 161–167.
[16] J. Obirai, T. Nyokong, Electrochim. Acta 50 (2005) 3296–3304.
[17] R. Baker, D.P. Wilkinson, J.J. Zhang, Electrochim. Acta 54 (2009) 3098–3102.
[18] F. Harnisch, S. Wirth, U. Schröer, Electrochem. Commun. 11 (2009) 2253–2256.
[19] G.I. Cárdenas-Jirón, M.A. Gulppi, C.A. Caro, R. delRío, M. Páez, J.H. Zagal, Electrochim. Acta 46 (2001) 3227–3235.
[20] C.J. Song, L. Zhang, J.J. Zhang, J. Electroanal. Chem. 587 (2006) 293–298.
[21] S. Iijima, Nature 354 (1991) 56–58.
[22] R.H. Baughman, A.A. Zakhidov, W.A. Heer, Science 297 (2002) 787–792.
[23] Y.P. Sun, K.F. Fu, Y. Lin, W.J. Huang, Acc. Chem. Res. 35 (2002) 1096–1104.
[24] J.F. Silva, S. Griveau, C. Richard, J.H. Zagal, F. Bedioui, Electrochem. Commun. 9 (2007) 1629–1634.
[25] A. Baba, Y. Kanetsuna, S. Sriwichai, Y. Ohdaira, K. Shinbo, K. Kato, S. Phanichphant, F. Kaneko, Thin Solid Films 518 (2010) 2200–2205.
[26] D.A. Geraldo, C.A. Togo, J. Limson, T. Nyokong, Electrochim. Acta 53 (2008) 8051–8057.
[27] M. Pomerantz, A. Aviram, R.A. McCorkle, L. Li, A.G. Schrott, Science 255 (1992) 1115–1118.
[28] C.Y. Tsai, S.P. Chen, T.C. Wen, Chem. Phys. 240 (1999) 191–196.
[29] B.H. Lee, J.Y. Jaung, S.C. Jang, S.C. Yi, Dyes Pigments 65 (2005) 159–167.
[30] D. Dini, M. Hanack, H.J. Egelhaaf, J.C. Sancho-García, J. Cornil, J. Phys. Chem. B 109 (2005) 5425–5432.
[31] Z.W. Xu, G.X. Zhang, Z.Y. Cao, J.S. Zhao, H.J. Li, J. Mol. Catal. A 318 (2010) 101–105.
[32] Z.W. Xu, H.J. Li, K.Z. Li, Y.H. kuang, Y.J. Wang, Q.G. Fu, Z.Y. Cao, W. Li, Cryst. Growth Des. 9 (2009) 4136–4141.
[33] J. Pillay, K.I. Ozoemena, Electrochim. Acta 52 (2007) 3630–3640.
[34] B. Ballesteros, G. Torre, C. Ehli, G.M. Aminur Rahman, F.A. Rueda, D.M. Guldi, T. Torres, J. Am. Chem. Soc. 129 (2007) 5061–5068.
[35] L. Cao, H.Z. Chen, H.Y. Li, H.B. Zhou, J.Z. Sun, X.B. Zhang, M. Wang, Chem. Mater. 15 (2003) 3247–3249.
[36] K. Wang, J.J. Xu, K.S. Tang, H.Y. Chen, Talanta 67 (2005) 798–805.
[37] A. Sivanesan, S. AbrahamJohn, Electrochim. Acta 53 (2008) 6629–6635.
[38] M. Kullapere, G. Jürmann, T.T. Tenno, J.J. Paprotny, F. Mirkhalaf, K. Tammeveski, J. Electroanal. Chem. 599 (2007) 183–193.
[39] R.E. Davis, G.L. Horvath, C.W. Tobias, Electrochim. Acta 12 (1967) 287–297.
[40] S. Choi, R. Choi, S.W. Han, J.T. Park, Chem. Commun. 46 (2010) 4950–4952.
[41] K. Tammeveski, K. Kontturi, R.J. Nichols, R.J. Potter, D.J. Schiffrin, J. Electroanal. Chem. 515 (2001) 101–112.
[42] G. Jürmann, K. Tammeveski, J. Electroanal. Chem. 597 (2006) 119–126.
[43] L. Qu, Y. Liu, J.B. Baek, L. Dai, ACS Nano 4 (2010) 1321–1326.
[44] N.R. Elezović, B.M. Babić, L.G. Krstajić, V. Radmilović, N.V. Krstajiće, L.J. Vračar, J. Power Sources 195 (2010) 3961–3968.
[45] H. Razmi, M. Agazadeh, B. Habibi-A, J. Electroanal. Chem. 547 (2003) 25–33.
[46] Z. Shi, J. Zhang, Z. Liu, H. Wang, D.P. Wilkinson, Electrochim. Acta 51 (2006) 1905–1916.
[47] H. Ding, X. Zhang, M.K. Ram, C. Nicolini, J. Colloid Interface Sci. 290 (2005) 166–171.
[48] Z. Dang, Y. Gao, H.P. Xu, J. Bai, J. Colloid Interface Sci. 322 (2008) 491–496.
[49] G.J. Yang, J.J. Xu, K. Wang, H.Y. Chen, Electroanalysis 18 (2006) 282–290.